J Solid State Electrochem (2010) 14:1279–1292
DOI 10.1007/s10008-009-0926-y

ORIGINAL PAPER

Analysis of the electrochemical quartz crystal microbalance response during oxidation of carbon oxides adsorption products on platinum group metals and alloys

Mariusz Łukaszewski · Hanna Siwek · Andrzej Czerwiński

Received: 12 May 2009 / Revised: 30 July 2009 / Accepted: 31 July 2009 / Published online: 16 September 2009

Abstract The analysis of the electrochemical quartz crystal microbalance (EQCM) signal is presented for the case of oxidation of carbon oxides adsorption products on Pt, Rh, and their alloys. It is demonstrated that the EQCM response can be roughly approximated by the mass balance involving adsorption/desorption of various species (carbon oxides, oxygen, anions, and water molecules) and metal dissolution. The results obtained by the EQCM are in good agreement with the electrochemical data and confirm the domination of CO radicals among the products of CO_2 reduction and CO adsorption on Pt-rich electrodes. In the case of Rh-rich electrodes, the existence of additional species (CHO or COH), more reduced than CO, is suggested.

Keywords Noble metals and alloys · CO_2 reduction · CO adsorption · Electrochemical quartz crystal microbalance · Apparent molar mass

Introduction

Since the 1980s, the electrochemical quartz crystal microbalance (EQCM) has been a widely used in situ technique for the investigation of various electrode processes. Its high sensitivity to mass changes allows for monitoring even submonolayer phenomena connected with adsorption, deposition, and dissolution (see [1–6] and references therein). However, one should be aware that apart from mass, there are other factors influencing the frequency of the quartz crystal resonator operating in liquid [1–18]. In fact, the EQCM is a kind of a non-selective sensor that responds to its nearest environment. In contact with the liquid phase, the EQCM is sensitive to the properties of adjacent solution on distances of the order of the velocity decay length of shear waves in liquid, i.e., about 250 nm for aqueous solutions [1]. Therefore, the analysis of the EQCM signal can sometimes be a real challenge for the investigators. Nevertheless, a proper application of the EQCM method coupled with careful data treatment can provide invaluable information regarding various processes occurring at the solid/liquid interface [1].

In the literature [2, 4], the data collected by the EQCM are often interpreted with the use of a parameter in units of grams per mole, called "apparent molar mass". This parameter can be obtained from a correlation between frequency change and charge consumed in a given electrode process, according to the equation:

$$\frac{M}{z} = -\frac{(\Delta f \times C \times F)}{Q} \tag{1}$$

where Δf is the measured frequency shift, C is the calibration constant of the quartz crystal resonator, F is the Faraday constant, z is the number of electrons exchanged, and Q is the charge passed.

Since more than one species can participate in the charge transfer reaction and some other species can additionally be adsorbed/desorbed without a charge transfer, the apparent molar mass is a resultant quantity of all those reactions. By a comparison of the experimental apparent molar mass with

M. Łukaszewski · A. Czerwiński (✉)
Department of Chemistry, Warsaw University,
Pasteura 1,
02-093 Warsaw, Poland
e-mail: aczerw@chem.uw.edu.pl

H. Siwek · A. Czerwiński
Industrial Chemistry Research Institute,
Rydygiera 8,
01-793 Warsaw, Poland

the value predicted on the basis of the assumed stoichiometry of the process studied, one can draw conclusions concerning the reaction mechanism. On the other hand, when other non-mass factors affect the frequency of a quartz crystal resonator, the measured value of *M/z* might not be equal to the difference between real molar masses of the species involved in the process examined. However, if the mass balance of the process is well defined, the deviation of the apparent molar mass from the real molar mass can be treated as a measure of those additional effects influencing the EQCM response (see, e.g., the studies on stress effects accompanying hydrogen absorption [19–21]). Therefore, the value of *M/z* can be a source of important information about the electrode reactions.

In this paper, we present the way of the analysis of the EQCM response in the process of oxidation of carbon oxides adsorption products on Pt, Rh, and their alloys (Pt-Rh, Pd-Pt, Pd-Rh, and Pd-Pt-Rh). These reactions are important in the context of better understanding and improvement of the work of direct methanol fuel cells, where CO_2 and CO are fuel oxidation products or intermediates (see [22–24] and references therein). CO_2 reduction and CO adsorption have already been investigated by many experimental techniques (see also our recent review [24]), e.g., infrared spectroscopy [25–31], radiochemistry [32–38], gas chromatography [39], mass spectrometry [40, 41], nuclear magnetic resonance [42, 43], and sum frequency generation [44]. However, the EQCM method was rather rarely applied in that subject [45–53] (mainly for studying CO adsorption on Pt), and no clear interpretation of the EQCM data exists in the literature. First attempts to analyze quantitatively the EQCM signal in carbon oxides adsorption experiments on platinum group metals and alloys have been presented in our earlier works [45–47, 53]. Here, we extend this approach and show how various factors influencing the resonator frequency contribute to the total measured frequency shift. With this paper, we continue our interest in the application of the EQCM method for the studies on electrochemistry of noble metals and their alloys [19–21, 45–47, 53–55].

Experimental

All experiments were performed at room temperature in 0.5 M H_2SO_4 solutions deoxygenated using an Ar stream. A $Hg|Hg_2SO_4|0.5$ M H_2SO_4 was used as the reference electrode. A Pt gauze was used as the auxiliary electrode. All potentials are recalculated with respect to the standard hydrogen electrode.

The EQCM M105 made by UELKO (Poland) was used together with an AUTOLAB potentiostat. Ten megahertz AT-cut Au-plated crystals (electrode geometric area 0.26 cm^2) produced by International Crystal Manufacturing were used in the EQCM experiments. The calibration constant determined by Ag and Pd deposition was 1.2 ng Hz^{-1}, very close to the theoretical value based on Sauerbrey equation [56].

Pt, Rh, and their alloys (Pt-Rh, Pd-Pt, Pd-Rh, and Pd-Pt-Rh) were deposited potentiostatically on Au surfaces as limited volume electrodes from baths containing respective chloride species ($PdCl_2$, H_2PtCl_6, $RhCl_3$, and HCl). Various compositions of the alloys were obtained by altering the deposition conditions (bath composition and deposition potential) as well as utilizing different dissolution rates of the metals during the procedure of potential cycling through the surface oxidation region [57, 58]. The thickness of metal/alloy layers was 0.2–0.3 μm. The roughness factor, as estimated from adsorbed hydrogen oxidation or surface oxide reduction charge [58], was ca. 40–150. All alloy compositions given in this work are surface compositions expressed in atomic percentages and were determined from the potential of the peak due to surface oxide reduction [57–61].

In the experiments with CO_2 reduction and CO adsorption, the gasses of 99.9% purity were used. During adsorption, the electrode was polarized at a constant potential, while the gas was introduced into the solution. After completing the adsorption and before recording cyclic voltammograms, CO_2 and CO were removed from the solution with Ar. The values of surface coverage and electron per site (eps) were calculated according to standard procedures [62–64].

Results and discussion

Factors influencing the EQCM response during the oxidation of reduced CO_2 and adsorbed CO—a model for data analysis

Figure 1 shows various types of current- and frequency-potential responses recorded during the oxidation of the products of CO_2 reduction and CO adsorption on Pd-Pt and Pd-Rh alloys. These curves are representative of Pt-based and Rh-based electrodes, respectively. The well-known cyclic-voltammetric (CV) characteristics are visible, namely the lowering in hydrogen desorption peaks (region 1 in Fig. 1) and the adsorbate oxidative stripping signal (I). In the course of the EQCM response, one should note the frequency decrease at CO_2 reduction/CO adsorption potential as compared with a clean electrode and the frequency drop during the adsorbate removal. These features have been discussed in detail in our earlier papers [45–47, 62, 63].

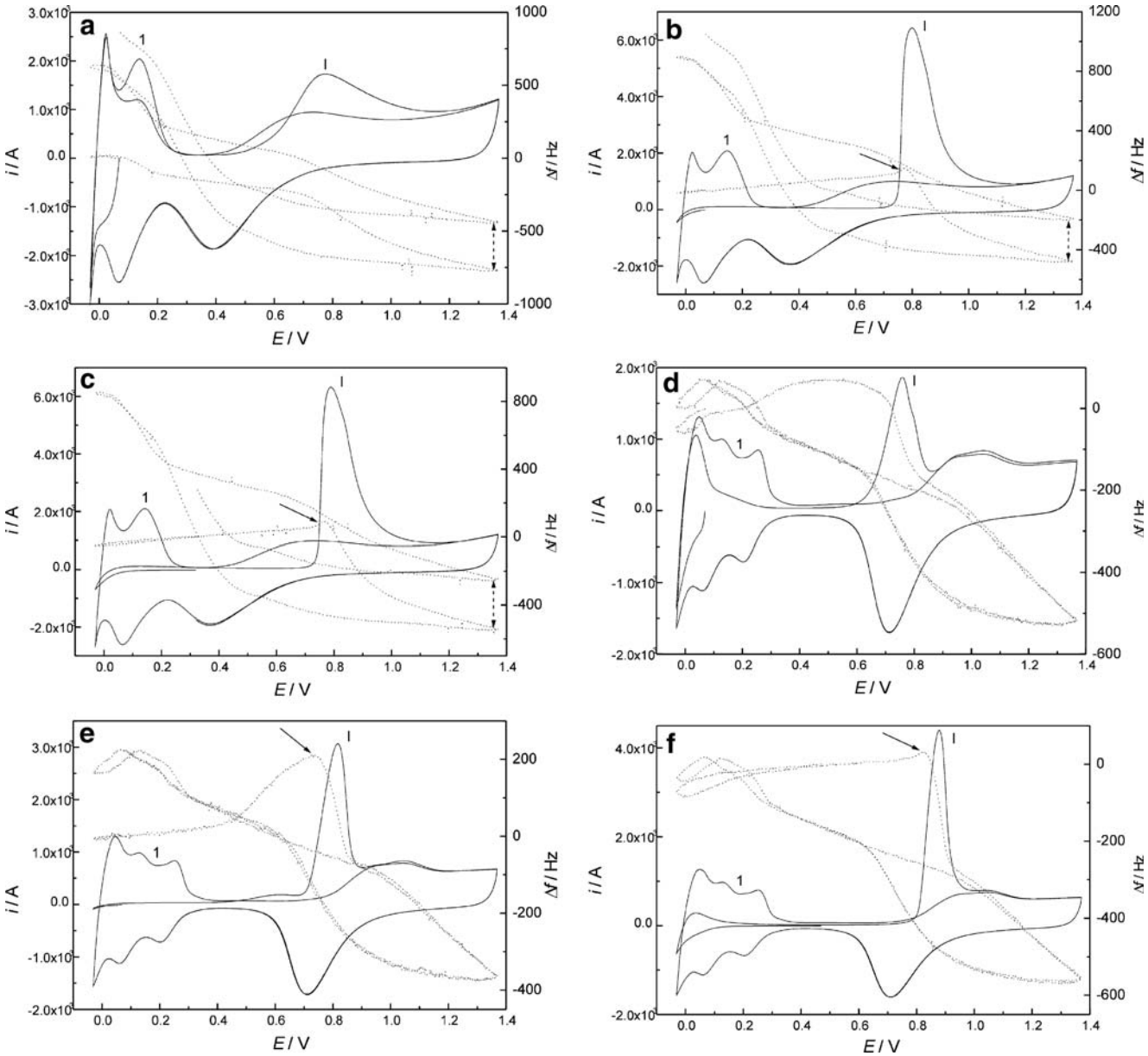

Fig. 1 Voltammetric and electrochemical quartz crystal microbalance responses during the oxidation of the products of CO_2 reduction (**a**, **d**) and CO adsorption (**b**, **c**, **e**, **f**) on: 14%Pd-Rh (**a**–**c**) and 60%Pd-Pt (**d**–**f**) alloy. Adsorption potentials: 0.07 V (**a**, **b**, **d**, **e**), 0.32 V (**c**), and 0.47 V (**f**)

From the frequency-to-charge ratio (Eq. 1) in the adsorbate oxidation region, we have obtained apparent molar mass (*M/z*) gain ranging from 3 to 6 g/mol for CO_2 and from 1 to 3 g/mol for CO. It should be stressed that if the EQCM could measure mass change solely due to reduced CO_2 or adsorbed CO removal, a mass loss (i.e., frequency rise) would be observed. Thus, the resultant mass increase (mirrored in frequency drop) confirms that the adsorbate oxidation is not the only electrode process occurring in this potential range. In fact, the adsorbate removal is accompanied by the electrode surface oxidation (i.e., surface oxide formation and metal dissolution) and water or anion readsorption. Thus, each of these reactions contribute to the mass balance determining the measured frequency change.

Since different structures of CO_2 reduction and CO adsorption products (denoted in the text as "the adsorbate") were postulated in the literature (mainly CO, COOH, COH, and CHO), a question arises whether these adsorbates can be distinguished by means of the EQCM experiment. To make such a comparison possible, one should know the *M/z* values expected for a given type of the adsorbate. Therefore, a formula predicting this parameter characteristic of various adsorbate structures must be obtained from a theoretical analysis of the factors influencing the EQCM response. Although it is questionable whether under our

experimental conditions the EQCM signal can be interpreted only gravimetrically [45–47], we believe that it is still possible to use the apparent molar mass as a kind of a mass equivalent to the measured frequency changes. In this approach, one may calculate the apparent molar mass change per number of electrons (M/z) for the oxidation of carbon oxides adsorption products taking into account mass and charge contributions from various electrode processes.

The first attempt to predict the EQCM response in carbon oxides adsorption experiment has been made in our recent paper [46], where we presented mass and charge balance involving adsorbed carbon oxides removal together with simultaneous surface oxide formation and anion and water readsorption:

$$\begin{aligned}&\theta\,\mathrm{M}_n\mathrm{CO}_x\mathrm{H}_y + n(1-\theta)\,\mathrm{M} + [(b+1)n + (2-x)\,\theta]\\ &\mathrm{H_2O} + an\,\mathrm{HSO_4^-} \rightarrow n\,\mathrm{MO}\left(\mathrm{HSO_4^-}\right)_a(\mathrm{H_2O})_b \\ &+\theta\,\mathrm{CO_2} + \{2[n + (2-x)\,\theta] + y\theta\}\,(\mathrm{H^+} + \mathrm{e^-})\end{aligned} \tag{2}$$

In this equation, n is the number of surface sites occupied by one molecule of the carbonaceous adsorbate, while x and y are stoichiometric factors in the general formula of the adsorbate (CO_xH_y). θ is the surface coverage with the adsorbate, which can be calculated from the ratio of the difference between the charges of adsorbed hydrogen oxidation in the absence and presence of reduced CO_2 or adsorbed CO $\left(\Delta Q^{\mathrm{ox}}_{\mathrm{Hads}}\right)$ to adsorbed hydrogen oxidation charge in the absence of these adsorbates $\left(Q^{\mathrm{ox}}_{\mathrm{Hads}}\right)$:

$$\theta = \frac{\Delta Q^{\mathrm{ox}}_{\mathrm{H_{ads}}}}{Q^{\mathrm{ox}}_{\mathrm{H_{ads}}}} \tag{3}$$

The coverages with adsorbed anions and water are denoted as a and b, respectively.

Another important effect that should be considered is mass loss due to metal dissolution, which proceeds in the potential range of reduced CO_2 or adsorbed CO oxidation. Metal dissolution was calculated from frequency difference between two consecutive anodic scans (as indicated by a dashed arrow in Fig. 1) and expressed as a fraction of a monolayer of surface atoms (k). Our earlier studies [54] on that subject have shown that under conditions applied, the maximum amount of dissolved metal equals to ca. 15% of monolayer for Pd, 4% for Rh, and 0.1% for Pt. For the alloys studied here, k was in the range 0–7% of a monolayer. The influence of metal dissolution effect on the experimental values of apparent molar mass change in the process of reduced CO_2 oxidation is demonstrated in Fig. 2.

According to the literature data on sulfate adsorption on Rh and Pt electrodes [65–69], we have taken the maximum change in surface coverage with anions (a) as

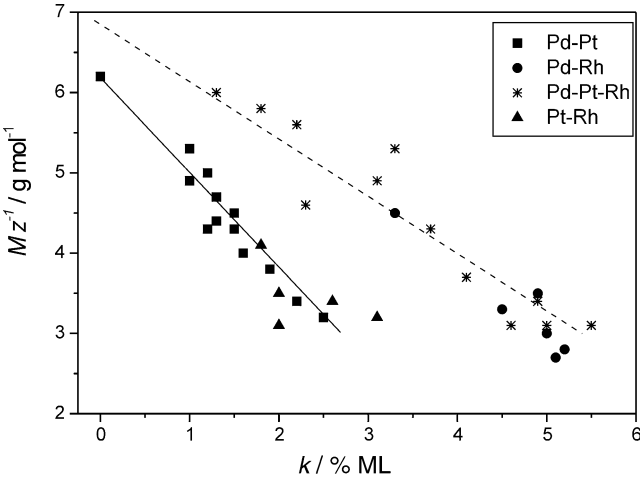

Fig. 2 Correlation between apparent molar mass change for the oxidation of reduced CO_2 and the extent of metal dissolution (expressed in percent of a monolayer)

0.1. The values of changes in water coverage are more difficult to define. One could assume that only water and anions compete for the surface sites vacated by reduced CO_2 or adsorbed CO, which means that the maximum change in surface coverage with water (b) is 0.9. However, since in the presence of reduced CO_2 and adsorbed CO partial water adsorption on surface sites free from the adsorbate is possible, a more justified assumption is $b=\theta-0.1$.

The stoichiometry of surface oxide is assumed to be 1:1, i.e., corresponding to the formula MO. This assumption is based on the analysis of the EQCM response for clean electrodes in the surface oxidation region. The values of apparent molar mass ranging from 5 to 8 g/mol for the anodic scan and 6–9.5 g/mol for the cathodic scan were obtained (Fig. 3). These values are close to 8 g/mol

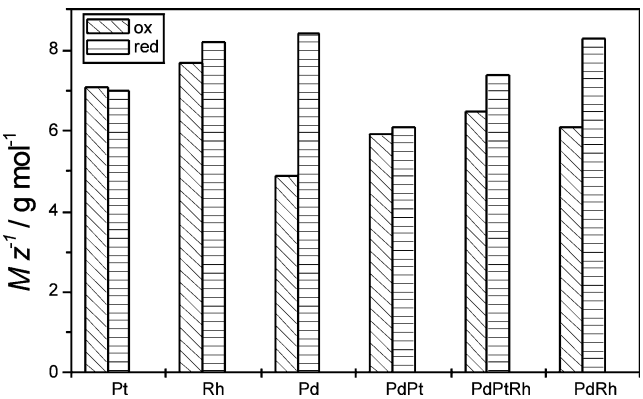

Fig. 3 Mean values of apparent molar mass change obtained for the processes of surface oxide formation (*ox*) and reduction (*red*) on platinum group metals and alloys

predicted for a two-electron reaction of surface oxide formation according to the scheme:

$$M + H_2O \rightarrow MO\ [16g] + 2H^+ + 2e^- \quad (4)$$

Thus, the theoretical *M/z* ratio for the process of reduced CO_2 or adsorbed CO oxidation can be obtained from the following relationship:

$$\frac{M}{z} = \frac{n[(1-k)(16 + a \times 97 + (\theta - a) \times 18) - k \times M_m] - \theta \times M_{CO_xH_y}}{2[n + 2(2-x)\theta] + y\theta} \quad (5)$$

Equations 2 and 5 were derived assuming that water and anions do not adsorb on the part of electrode covered with adsorbed carbon oxides. At first glance, it may be questioned, at least regarding water, as since the electrode is immersed in aqueous solution, water molecules must be present on the top of the adsorbate layer. In fact, however, their interactions with the electrode surface in the presence of adsorbed carbon oxides are much weaker than those with the bare metal, which is reflected on the fact that frequency decrease at adsorption potential is smaller than that predicted from the mass of the adsorbate itself [45–47]. This effect is equivalent to that corresponding to water desorption.

However, the above equation is based on some further assumptions: (1) a monolayer of surface oxide is formed simultaneously with the carbonaceous adsorbate oxidation; (2) in the presence of the carbonaceous adsorbate, water and anion adsorption is totally hindered also on surface sites free from the adsorbate; and (3) in the absence of the carbonaceous adsorbate, water and anions can be adsorbed on both the "metallic" and oxidized surface. In fact, a detailed analysis of voltammograms and the EQCM response reveal that these conditions are fulfilled only partially. Thus, the appropriate modifications of Eqs. 2 and 5 are necessary.

In the second approach [53], the above model has been modified taking into account the possibility of anion and water adsorption on the part of electrode surface not covered with adsorbed carbon oxides. Moreover, it should be noted that while on Rh and Rh-rich alloys a monolayer of surface oxide is completed during the carbonaceous adsorbate removal, on Pt and Pt-rich alloys, the adsorbate oxidation proceeds mainly in the double layer potential region, and only a fraction of a monolayer of surface oxide is formed. Therefore, an incomplete surface coverage with the oxide has been taken as a parameter (ϑ) in the modified equations (Eqs. 6 and 7). This value can be determined from the charge in the surface oxidation region on CV curves recorded for clean electrodes. Additionally, according to some literature data [70], the anion and water desorption after surface oxide formation has to be taken into account. This approach yields the following total mass balance during the adsorbate oxidation and the related expected *M/z* ratio [53]:

$$\begin{aligned} &\theta\, M_nCO_xH_y + n(1-\theta)\, M\left(HSO_4^-\right)_a(H_2O)_b \quad (6)\\ &+\{n[\vartheta(1-b) + \theta b] + \theta(2-x)\}\, H_2O + [an(\theta - \vartheta)]\, HSO_4^- \rightarrow \\ &\rightarrow n\, MO + \theta\, CO_2 + n(1-\vartheta)M\left(HSO_4^-\right)_a(H_2O)_b \\ &+\{2n\vartheta + \theta[y + 2(2-x)]\}\, (H^+ + e^-) \end{aligned}$$

$$\frac{M}{z} = \frac{[n\vartheta \times 16 + n(1-\vartheta)(a \times 97 + b \times 18) - k \times M_m] - \left[\theta \times M_{CO_xH_y} + n(1-\theta)(a \times 97 + b \times 18)\right]}{2n\vartheta + \theta[y + 2(2-x)]} \quad (7)$$

As will be demonstrated below (next section), the first model (Eq. 5) works much better for Rh than for Pt, although in both cases, it leads to overestimated *M/z* values. On the other hand, the second model (Eq. 7) can be successfully applied to Pt, but in the case of Rh, the predicted *M/z* values are much lower than the experimental ones. Therefore, an attempt has been made to establish a new model based on some elements of both previous models and with a stronger experimental support for the assumptions made.

The main modifications in Eq. 6 are different values of surface coverage with anions and water for different states of the electrode surface. First, from the analysis of the EQCM response for clean electrodes in the hydrogen and double layer potential regions, a maximum surface coverage with anions could be obtained. These calculations were done in two ways:

1. From the mass balance during hydrogen desorption:

$$MH + a\, HSO_4^- \rightarrow M\left(HSO_4^-\right)_a + H^+ + e^- \quad (8)$$

hence

$$a = \frac{\left(\frac{M}{z} + 1\right)}{97} \quad (9)$$

where *M/z* is the experimental value of apparent molar mass per number of electrons, obtained from $\Delta f/Q$ ratio.

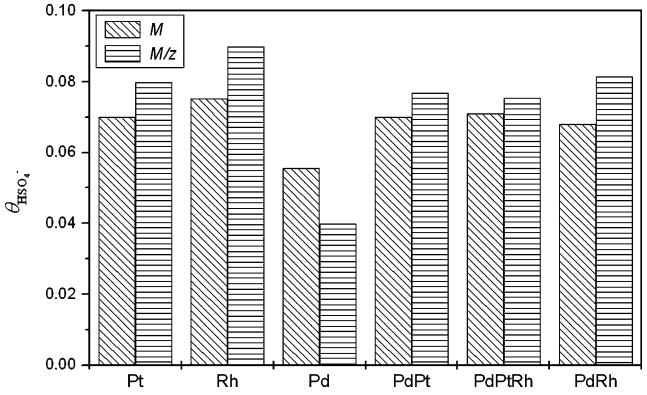

Fig. 4 Surface coverage with HSO_4^- anions obtained from apparent molar mass changes according to Eq. 9 (*M/z*) and Eq. 11 (*M*)

2. From the mass gain (Δm) determined from frequency decrease in the hydrogen and double layer regions, related to the number of surface sites (n')

$$M = \frac{\Delta m}{n'} \tag{10}$$

$$a = \frac{M}{97} \tag{11}$$

In both cases, a mean coverage with anions (a) of 0.07 was obtained (Fig. 4). This value was further assumed for the surface coverage with anions on the "metallic" (i.e., not covered with adsorbed carbon oxides or surface oxide) part of the electrode. Assuming that only water and anions compete for the surface sites vacated by reduced CO_2 or adsorbed CO, maximum coverage with adsorbed water was taken as $b=1-a$, i.e., 0.93 for a clean electrode.

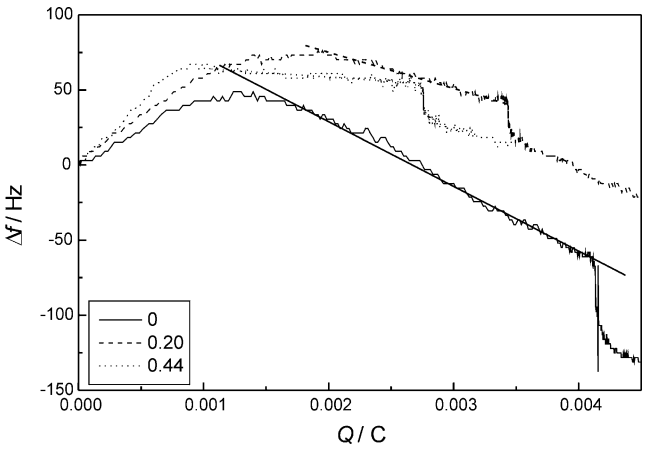

Fig. 5 Frequency change vs charge in the process of hydrogen desorption for various values (indicated in the legend) of surface coverage of a Pd-Rh alloy with reduced CO_2

Second, since in the literature [71] there are premises that in the presence of surface oxide, only a partial desorption of sulfates occurs and some surface sites still remain occupied by the anions, in the next approach to the EQCM data interpretation, a lower coverage with anions (A) was assumed (0.03) for the oxidized part of the electrode surface. This value was obtained by ascribing the difference between the mean apparent molar mass change per number of electrons during surface oxidation (i.e., 6.4 g/mol) and the value expected for 2-electron reaction of MO formation (8 g/mol) to the effect of the partial removal of adsorbed anions. The possibility of water adsorption on the electrode covered with surface oxide was also reported in the literature [71].

On the other hand, the lowering in the slope of frequency-charge relationship in the hydrogen region in the presence of reduced CO_2 (Fig. 5) suggests that under these conditions, water and anion adsorption is partially suppressed also on surface sites free from the adsorbate. However, due to a different molecular size, the steric effects should be much more pronounced in the case of HSO_4-anions than for water. As demonstrated in Fig. 6, with the increase in the coverage with reduced CO_2, the apparent molar mass for desorption of adsorbed hydrogen decreases. Therefore, surface coverage with anions (α) and water (β) on the part of the electrode not covered with reduced CO_2 or adsorbed CO have been assumed to depend linearly on surface coverage with the carbonaceous adsorbate:

$$\alpha = a(1-\theta) \tag{12}$$

$$\beta = b(1-\theta) + \theta \tag{13}$$

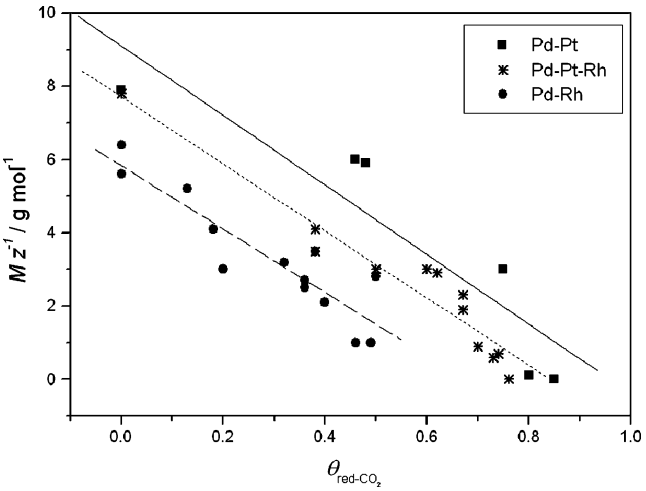

Fig. 6 Apparent molar mass changes in the process of hydrogen desorption vs surface coverage with reduced CO_2

Finally, it was found in our recent paper [55] that Pd dissolution leads to the formation of Pd^{2+} ions, while Rh is oxidized mainly to Rh^{3+} ions. Therefore, in the latter case, the change in metal valency (Δz) due to its dissolution as compared with the valency in metal oxide (+II) should be taken into account.

On the basis of the above considerations, the following mass and charge balance is obtained (Eq. 14) together with the formula for the apparent molar mass change per number of electrons (Eq. 17) in the process of adsorbed carbon oxides removal:

$$\begin{aligned}&\theta\, M_nCO_xH_y + n(1-\theta)\, M\left(HSO_4^-\right)_\alpha(H_2O)_\beta \\ &+[n\vartheta + \theta(2-x) + \Delta_b]\, H_2O + \Delta_a\, HSO_4^- \rightarrow \\ &\rightarrow \vartheta n\, MO\left(HSO_4^-\right)_A(H_2O)_B + \theta\, CO_2 \\ &+ n(1-\vartheta)M\left(HSO_4^-\right)_a(H_2O)_b \\ &+\{2n\vartheta + \theta[y + 2(2-x)]\}\ (H^+ + e^-)\end{aligned} \tag{14}$$

where:

$$\Delta_a = n(\vartheta A + a - \vartheta a - \alpha + \theta\alpha) \tag{15}$$

$$\Delta_b = n(\vartheta B + b - \vartheta n - \beta + \theta\beta) \tag{16}$$

$$\frac{M}{z} = \frac{n[(1-k)[\vartheta(16 + A\times 97 + B\times 18) + (1-\vartheta)(a\times 97 + b\times 18)] - kM_m] - \left[\theta M_{CO_xH_y} + n(1-\theta)(\alpha\times 97 + \beta\times 18)\right]}{2\vartheta n + \theta[y + 2(2-x)] + nk\times\Delta z} \tag{17}$$

A comparison between various ways of the analysis of the EQCM response for reduced CO_2 oxidation

Equations 5, 7, and 17 enable to calculate *M/z* values for different structures of carbon oxides adsorption products (i.e., for different *x*, *y*, and *n*), for a given set of experimental parameters, i.e., surface coverage with the carbonaceous adsorbate (θ), surface coverage with surface oxide (ϑ), and the extent of metal dissolution (*k*). Figure 7 shows the influence of θ and ϑ on the *M/z* values (for k=0) for six possible adsorbates, i.e., MCO, M_2CO, MCOOH, MCOH (or MCHO), M_2COH, and M_3COH calculated according to Eq. 17. It should be noted that in order to better distinguish between various adsorbates, possibly high θ and low ϑ should be applied. For this combination of these parameters, the differences in *M/z* values between various structures are more pronounced. However, in practice, the choice of such advantageous experimental conditions is rather limited. Although for CO_2 adsorption on Pt and Pt-rich alloys these requirements can be well fulfilled, this is no longer the case for Rh-rich electrodes. For the latter system, a relatively low coverage with the adsorbate is accompanied by a wide potential range of its oxidation overlapping with surface oxide formation and, therefore, *M/z* parameter is less specific about the nature of the adsorbate. Nevertheless, as will be demonstrated below, from the comparison of the obtained *M/z* values with the experimental results, some important conclusions can be drawn concerning the adsorbate composition and structure.

The *M/z* ratio is very sensitive to the extent of metal dissolution (see Fig. 2), therefore in all the subsequent calculations, the metal dissolution factor was determined independently from the experimental data for each value of the calculated apparent molar mass. Thus, the real mass change due to the dissolution effect is involved in each theoretical value of *M/z* predicted by our model, and no approximations need to be made. The values of surface coverage with anions determined from Eq. 11 for various types of electrodes differed by ca. 7% of the relative value for pure Pt and Rh and by no more than 3% for the alloys, which gives the differences in *M/z* ratio not exceeding ca. 0.3 g/mol.

Since the three presented ways of the EQCM data analysis differ in respect of the assumptions made, they lead to different *M/z* values. To verify the usability of these equations for the determination of the nature of the adsorbate, the calculated apparent molar mass has to be compared with the experimental values for well-defined systems, such as pure metals: Pt and Rh.

Figure 8 presents theoretical *M/z* values predicted for the oxidation of various CO_2 reduction products together with experimental results, for Pt and Rh. It is evident that for all single structures, there are differences between the calculated and experimental *M/z* values. However, this behavior can be explained by the fact that the product of CO_2 reduction is not homogeneous, i.e., it consists of at least

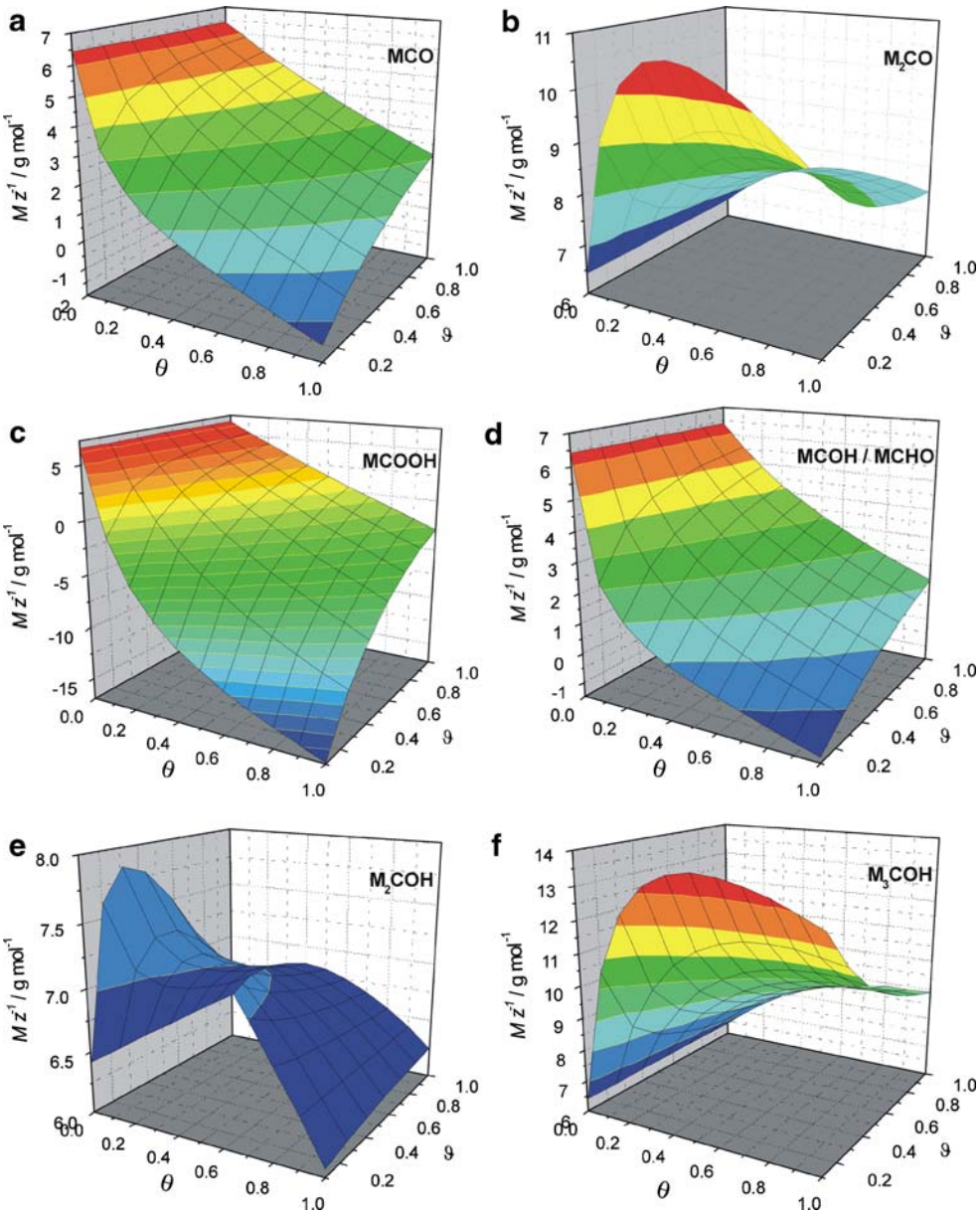

Fig. 7 Apparent molar mass changes calculated from Eq. 17 as a function of surface coverage with the carbonaceous adsorbate (θ_{ads}) and surface oxide (θ_O) for various adsorbates: (**a**) MCO, (**b**) M_2CO, (**c**) MCOOH, (**d**) MCHO/MCOH, (**e**) M_2COH, and (**f**) M_3COH

two kinds of species. In that case, the experimental *M/z* value for such a mixture should be intermediate between the values for the respective pure components. Careful analysis of the data shown in Fig. 8 reveals that these conditions are not always fulfilled. In case 3 for Pt and cases 2 and 3 for Rh, the experimental *M/z* value is higher than any value corresponding to a particular structure. It suggests that not all the approaches to the EQCM data treatment are in agreement with the experiment. These qualitative conclusions are supported by the analysis of electron per site (*eps*) values obtained from the electrochemical data, which were 1.20 for Pt and 2.24 for Rh. Assuming that the adsorbate is a mixture of two products characterized by two different *eps* values, the experimental *eps* is given as:

$$eps = eps_1 \cdot x_1 + eps_2 \cdot (1 - x_1), \tag{18}$$

and thus the fraction of surface sites occupied by a given product (x_1) can be calculated according to the equation:

$$x_1 = \frac{(eps - eps_2)}{eps_1 - eps_2} \tag{19}$$

where *eps* is the experimental value, while eps_1 and eps_2 are the theoretical values for product 1 and 2, respectively. Once the relative contributions from various products have been established, it is possible to calculate *M/z* values for different binary mixtures of the adsorbates and then compare them with the experimental data. Such results are shown in Fig. 9. It can be seen that for Pt in most cases, the best agreement between our models and the experiment is obtained for the adsorbate composed of linearly and bridge-bonded CO species (*eps*=2 and 1, respectively). However, the still higher

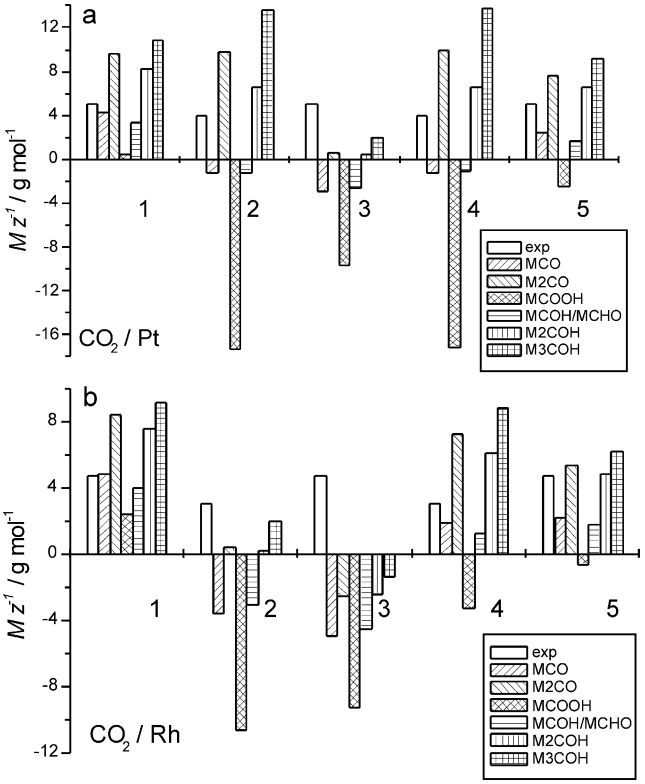

Fig. 8 Apparent molar mass changes obtained experimentally and calculated for different adsorbates for reduced CO_2 oxidation on Pt (**a**) and Rh (**b**). Numbers denote the following conditions used in the calculations: *1*, Eq. 5, k=0 for Pt and 3.8 for Rh; *2*, Eq. 7, ϑ=0.06, k=0 for Pt and 0.45, 1.2 for Rh; *3*, Eq. 7, ϑ=0.85, k=0 for Pt and 1.0, 3.8 for Rh; *4*, Eq. 17, ϑ=0.06, k=0 for Pt and 0.45, 1.2 for Rh; *5*, Eq. 17, ϑ=0.85, k=0 for Pt and 1.0, 3.8 for Rh. Other parameters: θ=0.83 for Pt and 0.48 for Rh, *eps*=1.20 for Pt and 2.24 for Rh

calculated *M/z* values in comparison with the experimental ones can suggest the additional existence of COOH radicals (but no more than 15% of the total amount of the adsorbate characterized by *eps*=1). On the other hand, the results for Rh indicate the existence of CHO (*eps*=3) or COH ($1 \le eps \le 3$, depending on the number of surface sites occupied by one molecule of the adsorbate) radicals among the products of CO_2 adsorption. This finding is in line with earlier reports [29, 64] that after CO_2 adsorption on Rh-based electrodes, species more reduced than CO are present.

It should be noted, however, that in case 3 for Pt and cases 2 and 3 for Rh, a great divergence between model and experiment is observed, i.e., the calculated *M/z* values are generally too low. Therefore, the approach based on Eq. 7 is not satisfactory, especially for Rh. Also, for Pt, the calculations based on Eq. 5 yield overestimated *M/z* values (case 1). This is because in this approach, a full monolayer of surface oxide is assumed, which is far from real conditions. Thus, Eq. 5 works only for Rh electrode, where reduced CO_2 oxidation signal is strongly overlapped with surface oxide formation currents. On the other hand, the model based on Eq. 17 can be successfully applied for both Pt and Rh and therefore seems to be the most promising.

Equation 17 was further used for the analysis of the EQCM data for reduced CO_2 oxidation on Pt and Rh alloys (Fig. 10). Again, for Pd-Pt and Pt-Rh alloys, the best agreement between our model and the experiment is obtained for the adsorbate composed of linearly and bridge-bonded CO species, possibly with an addition of small amounts of COOH radicals, while for Rh-based alloys (Pd-Rh and Pd-Pt-Rh), a significant contribution from CHO or COH radicals can be suggested.

One could suppose that trying to identify the composition of the adsorbed species (CO vs CHO or COH), which may differ by only one hydrogen atom, from the mass-to-charge balance is rather uncertain and falls into the error margins. However, it should be stressed here that the factor which is analyzed is not the molar mass alone but the ratio between the mass and charge (*M/z*), and due to different number of electrons exchanged (2 vs 3), this value differs more for CO and COH/CHO than the molar masses alone. Moreover, another important factor which affects the value of *M/z* is the number of surface sites occupied by one molecule of the

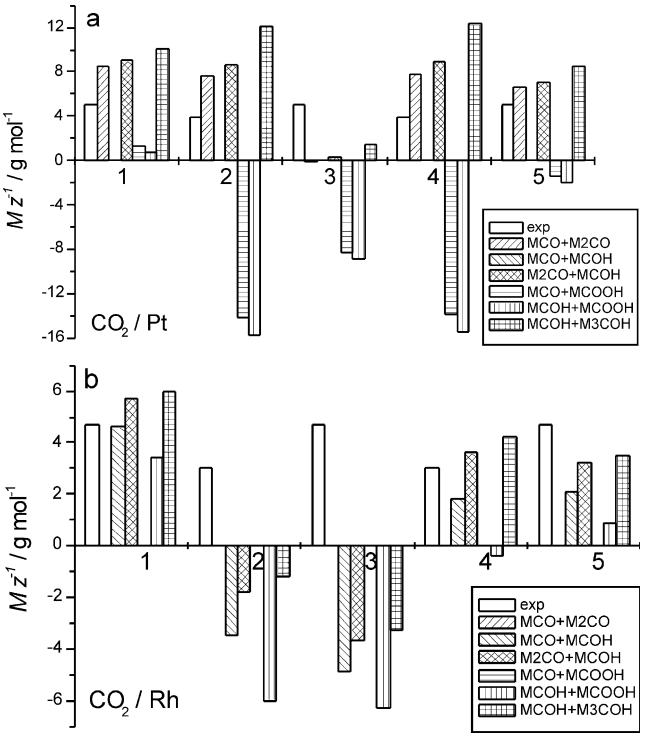

Fig. 9 Apparent molar mass changes obtained experimentally and calculated for different binary mixtures of adsorbates for reduced CO_2 oxidation on Pt (**a**) and Rh (**b**). Numbers denote the following conditions used in the calculations: *1*, Eq. 5 k=0 for Pt and 3.8 for Rh; *2*, Eq. 7, ϑ=0.06, k=0 for Pt and 0.45, 1.2 for Rh; *3*, Eq. 7, ϑ=0.85, k=0 for Pt and 1.0, 3.8 for Rh; *4*, Eq. 17, ϑ=0.06, k=0 for Pt and 0.45, 1.2 for Rh; *5*, Eq. 17, ϑ=0.85, k=0 for Pt and 1.0, 3.8 for Rh. Other parameters: θ=0.83 for Pt and 0.48 for Rh, *eps*=1.20 for Pt and 2.24 for Rh

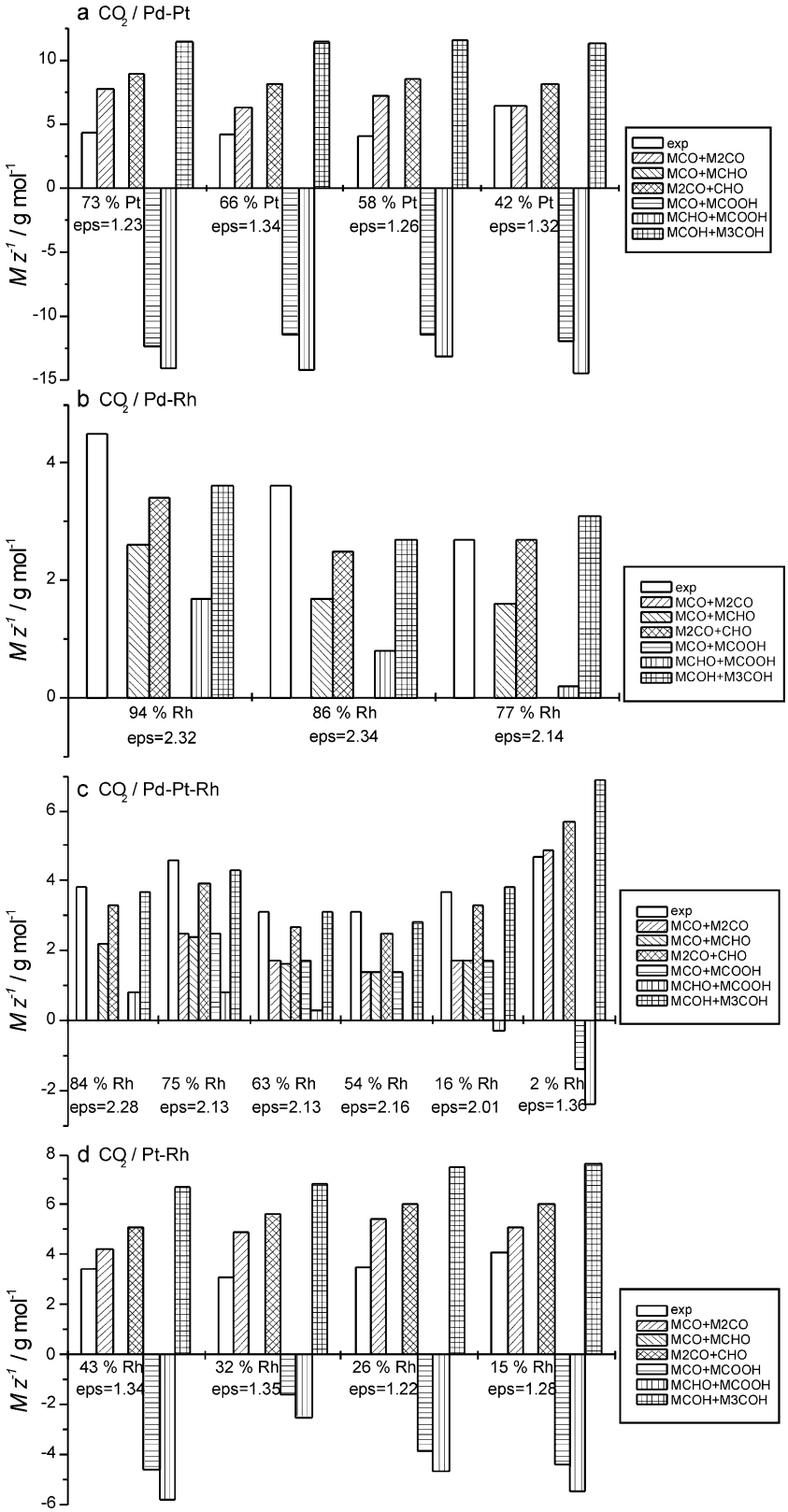

Fig. 10 Apparent molar mass changes obtained experimentally and calculated (Eq. 17) for different binary mixtures of adsorbates for reduced CO_2 oxidation (adsorption potential 0.02 V) on alloys of various surface compositions: (**a**) Pd-Pt, (**b**) Pd-Rh, (**c**) Pd-Pt-Rh, and (**d**) Pt-Rh

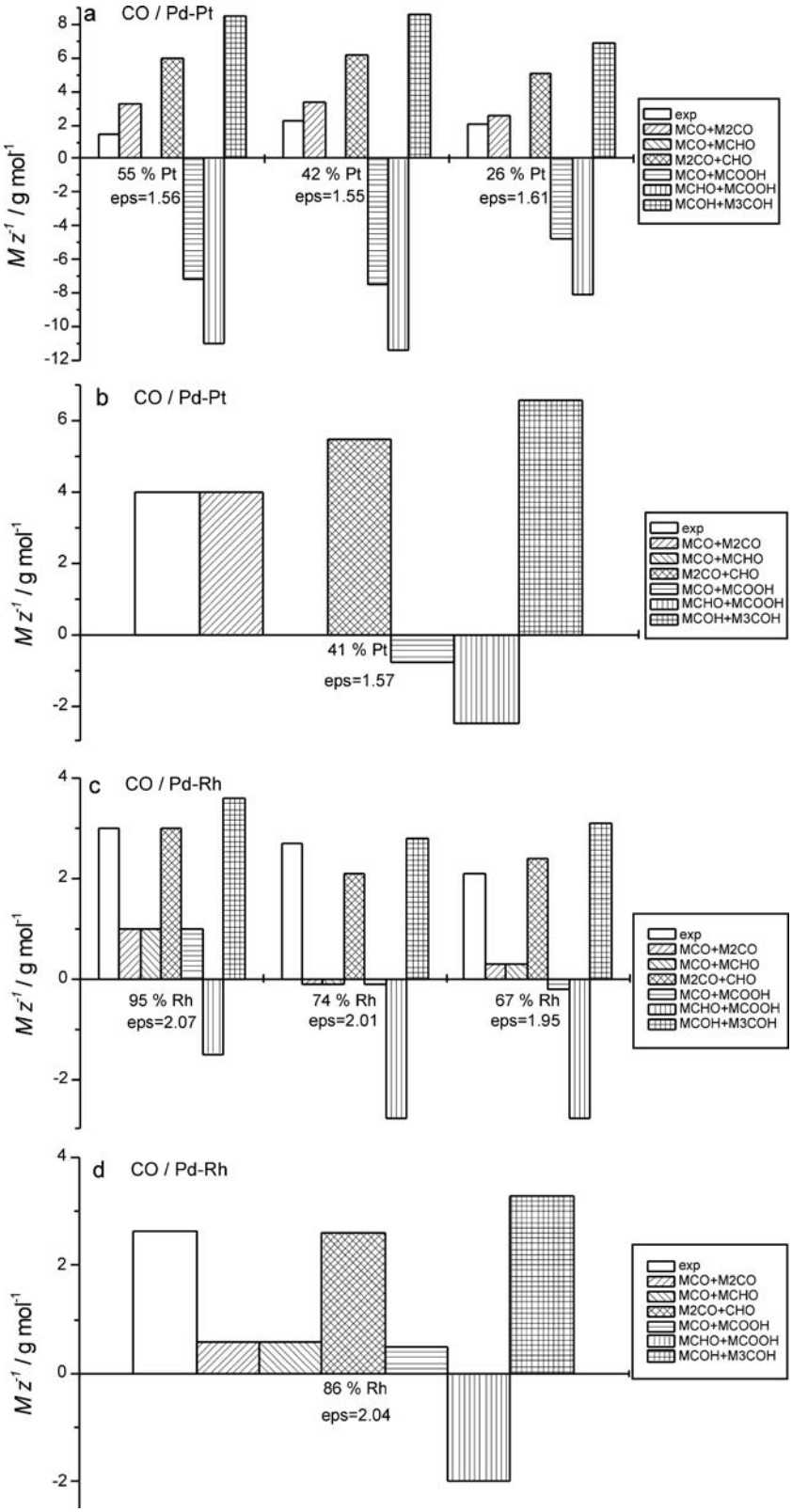

Fig. 11 Apparent molar mass changes obtained experimentally and calculated (Eq. 17) for different binary mixtures of adsorbates for adsorbed CO oxidation on alloys of various surface compositions: (**a**) Pd-Pt, adsorption potential 0.07 V, (**b**) Pd-Pt, adsorption potential 0.47 V, (**c**) Pd-Rh, adsorption potential 0.07 V, and (**d**) Pd-Rh, adsorption potential 0.32 V

adsorbate (n), see Eq. 17. For CO species, this value may be 1 or 2, which corresponds to linearly and bridge-bonded CO, respectively, while for COH, it may be 1, 2, or 3. For each combination of molar mass, z, and n values, different M/z values are obtained which allow to distinguish between various types of the adsorbate. Furthermore, the independent information on the adsorbed species was obtained from the aforementioned analysis of *eps* values. Figures 9 and 10 clearly demonstrate that using the model based on Eq. 17, it is possible to discriminate between a mixture of CO radicals and a mixture of COH/CHO radicals of various types of bonding with the surface. Other arguments for the presence of CHO or COH radicals among the products of CO_2 reduction on Rh-based electrodes were presented in our earlier paper [47].

Analysis of the EQCM response for adsorbed CO oxidation

The model based on Eq. 17 can also be used for the EQCM data analysis during the oxidation of adsorbed CO. However, in comparison with the case of CO_2, surface coverage with adsorbed CO is much higher, and its maximum value can reach almost a full monolayer. Therefore, the difference between two electrode states, i.e., in the presence and absence of the adsorbate, is greater than for reduced CO_2. On the one hand, this fact is favorable due to a higher contribution from the effect of the mass change of the adsorbate removal to the overall measured frequency shift. On the other hand, however, it means that for adsorbed CO oxidation, the non-mass effects can be more important than for reduced CO_2 oxidation. CO is known to both displace and co-adsorb water, whose amount depends on the adsorbate coverage [72]. These interactions are mirrored in the course of frequency-potential response in the hydrogen and double layer regions, where in the presence of the adsorbate, a frequency rise is observed, which is not adequate to the mass change due to the adsorbate removal. It was suggested in the literature [51] that with increasing potential (and increasing positive charge of the electrode), water molecules present on top of the adsorbate layer are being repulsed, which leads to weaker mutual interactions and therefore to a frequency increase. This effect is particularly well-pronounced in the case of CO adsorption on Pt electrode at potential in the hydrogen adsorption region, where a rapid frequency increase during the removal of the more easily oxidizable part of the adsorbate is observed. These effects have been thoroughly discussed elsewhere [45–47].

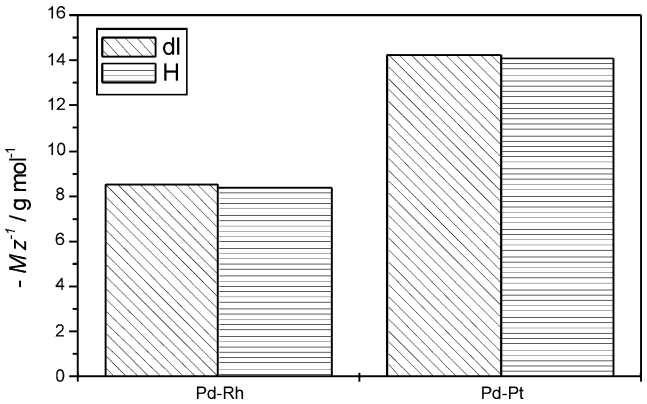

Fig. 12 Apparent molar mass changes obtained for the initial stage of the oxidation of CO adsorbed at potentials from the double layer (dl) and hydrogen (H) regions on Pd-Rh and Pd-Pt alloys

Bearing in mind the above limitations of the gravimetric approach to the EQCM data interpretation, an attempt has been made to apply Eq. 17 to the analysis of the EQCM response during adsorbed CO oxidation on Pd-Pt and Pd-Rh alloys (Fig. 11). In general, the conclusions drawn for CO adsorption are similar to the findings for reduced CO_2 oxidation, i.e., the domination of CO and CHO or COH species can be suggested for Pt-based and Rh-based electrodes, respectively. However, it should be stressed that the relative proportions between the particular adsorbates are different than in the case of CO_2 adsorption, as mirrored in different *eps* values. For Rh-rich electrodes, *eps* values for CO adsorption are lower than for CO_2 reduction, while for Pt-based alloys, an opposite relation is observed. It means that the adsorption products of CO_2 reduction on those alloys are not totally identical with the products of a direct CO adsorption. The problem of similarities and differences between these adsorbates has been widely discussed in our recent papers [46, 47].

It should be added that in the case of *eps* values close to 2, observed for Pd-Rh alloys, suggesting the existence of exclusively linearly bonded CO, the comparison of the calculated and experimental M/z values indicates rather a mixture of bridge-bonded CO and CHO or COH radicals. Thus, from the EQCM signal, it is possible to obtain some additional information on the nature of the adsorbate, which could not be extracted from the electrochemical data alone.

A careful analysis of the EQCM response during adsorbed CO oxidation reveals that at the very beginning of the adsorbate stripping, a frequency increase is observed (indicated by a solid arrow in Fig. 1), followed by a subsequent frequency drop. This behavior suggests that at the initial stage of the adsorbate oxidation, the EQCM detects mainly the mass loss due to adsorbed CO removal. Since CO coverage is high, water and anion adsorption is probably suppressed because of streric effects. Anions and water can be readsorbed only after the electrode surface is partly liberated from the carbonaceous adsorbate. A similar sequence of frequency changes was observed during chronoamperometric experiments [47, 73]. Therefore, by the analysis of this initial part of CV and frequency-potential curve, it may be possible to separate from the

EQCM signal the contribution originating mainly from the adsorbate oxidation. Under these conditions, the mass and charge balance can be assumed as:

$$M_nCO_xH_y + (2-x)\,H_2O \rightarrow CO_2 + (4-2x+y)\,[H^+ + e^-] + nM \quad (20)$$

and *M/z* ratio can be calculated as:

$$\frac{M}{z} = -\frac{M_{CO_xH_y}}{(4-2x+y)} \quad (21)$$

As shown in Fig. 12, the experimental *M/z* values for initial stages of CO oxidation were close to −14 g/mol for Pd-Pt alloys and ca. −9 g/mol for Pd-Rh alloys. These values suggest dominant oxidation of CO molecules in the former case and CHO or COH radicals in the latter case. Thus, this analysis confirms the above results that the products of CO adsorption on Pt- and Rh-based electrodes are different.

Interestingly, in contrast to adsorbed CO oxidation, the frequency rise could not be observed at any stage of reduced CO_2 oxidation. This can be explained by a lower surface coverage with the latter adsorbate. Probably in that case, due to lateral interactions, anions and water have much easier access to the part of electrode surface being liberated from the carbonaceous species, and therefore, the effect of their adsorption obscures the effect of the adsorbate removal.

The above results demonstrate that it is possible to establish a model for quantitative analysis of the EQCM response in the experiments with carbon oxides adsorption and oxidation of their adsorption products on platinum group metals and their alloys. Nevertheless, one should always remember that in the gravimetric approach to the EQCM data analysis, the non-mass effects are neglected. In the case of carbon oxide adsorption, the most important additional effects concern the changes in the interactions at the metal-solution interface during the adsorbate oxidation. These factors may be different for different structures of the adsorption products, especially for species of different polarity, which probably affects the strength of their interactions with water molecules from the solution (see discussion in [46, 47]). If we assume in the first approximation that the strength of the interactions between the adsorbate and water molecules is determined by the values of dipole moment and the ability to create hydrogen bonds, such polar structures as COOH, COH, and CHO should lead to a substantial frequency change exceeding a pure mass effect, while less polar species, such as CO, are expected to exhibit a weaker effect. However, further work is needed to establish the influence of such effects on the EQCM response and to help us to understand better the complex electrode processes occurring in carbon oxides adsorption experiments on platinum group metals and alloys.

Conclusions

The EQCM response during the oxidation of the products of CO_2 reduction and CO adsorption on Pt, Rh, and their alloys can be roughly approximated by the mass and charge balance involving the following parameters: (1) surface coverage of the electrode with the carbonaceous adsorbate; (2) surface coverage with the oxide (adsorbed oxygen); (3) surface coverage with anions and water for a clean metallic surface, in the presence of the carbonaceous adsorbate and in the presence of surface oxide; and (4) the extent of metal dissolution. All these parameters can be determined from the analysis of CV curves in the presence and absence of carbon oxides adsorption products, utilizing the respective charge and frequency responses.

By careful data treatment, analyzing the values of apparent molar mass (*M/z*) determined from frequency-charge correlation for the process of adsorbed carbon oxides oxidation, it is possible to obtain some information on the nature of these adsorbates. The EQCM results are consistent with the conclusions drawn on the basis of other methods that the adsorbate is a mixture of mainly linearly and bridge-bonded CO molecules, together with a small addition of COOH radicals on Pt-rich electrodes and with a significant contribution from CHO or COH radicals in the case of Rh-rich electrodes.

References

1. Tsionsky V, Daikhin L, Urbakh M, Gileadi E (2004) In: Bard AJ, Rubinstein I (eds) Electroanalytical chemistry. A series of advances, vol 22. Marcel Dekker, New York, p 2
2. Hepel M (1999) In: Wieckowski A (ed) Interfacial electrochemistry. Marcel Dekker, New York, p 599
3. Buttry DA, Ward MD (1992) Chem Rev 92:1355
4. Buttry DA (1991) In: Bard AJ (ed) Electroanalytical chemistry. A series of advances, vol 17. Marcel Dekker, New York, p 1
5. Schumacher R (1990) Angew Chem Int Ed Engl 29:329
6. Deakin MR, Buttry DA (1989) Anal Chem 61:1147A
7. Thompson M, Kipling AL, Duncan-Hewitt WC, Rajaković L, Čavić-Vlasak BA (1991) Analyst 116:881
8. Urbakh M, Daikhin L (1994) Phys Rev B 49:4866
9. Daikhin L, Gileadi E, Katz G, Tsionsky V, Urbakh M, Zagidulin D (2002) Anal Chem 74:554
10. Urbakh M, Daikhin L (1994) Langmuir 10:2836
11. Martini SJ, Frye GC (1993) Anal Chem 65:2910
12. Daikhin L, Urbakh M (1997) Faraday Discuss 107:27
13. Bund A, Schneider O, Dehnke V (2002) Phys Chem Chem Phys 4:3552
14. Daikhin L, Urbakh M (1996) Langmuir 12:6354
15. Gordon JS, Johnson DC (1994) J Electroanal Chem 365:267
16. Kanazawa KK, Gordon JG (1985) Anal Chim Acta 175:99
17. Lin Z, Ward MD (1995) Anal Chem 67:685
18. McHale G (2000) J Appl Phys 88:7304
19. Grdeń M, Kotowski J, Czerwiński A (1999) J Solid State Electrochem 3:348
20. Grdeń M, Kuśmierczyk K, Czerwiński A (2002) J Solid State Electrochem 7:43

21. Łukaszewski M, Czerwiński A (2006) J Electroanal Chem 589:87
22. Ralph TR, Hogarth MP (2002) Platin Met Rev 46:117
23. de Bruijn FA, Papageorgos DC, Sitters EF, Janssen GJM (2002) J Power Sources 110:117
24. Łukaszewski M, Siwek H, Czerwiński A (2009) J Solid State Electrochem 13:813
25. Beden B, Bewick A, Razaq M, Weber J (1982) J Electroanal Chem 139:203
26. Huang H, Fierro C, Scherson D, Yeager EB (1991) Langmuir 7:1154
27. Arévalo MC, Gomis-Bas C, Hahn F, Beden B, Arévalo A, Arvía AJ (1994) Electrochim Acta 39:793
28. Marcos ML, González-Velasco J, Hahn F, Beden B, Lamy C, Arvía AJ (1997) J Electroanal Chem 436:161
29. Arévalo MC, Gomis-Bas C, Hahn F (1998) Electrochim Acta 44:1369
30. Smolinka T, Heinen M, Chen YX, Jusys Z, Lehnert W, Behm RJ (2005) Electrochim Acta 50:5189
31. Beden B, Lamy C, de Tacconi NR, Arvia A (1990) Electrochim Acta 35:691
32. Urbach HB, Adams LG, Smith RE (1974) J Electrochem Soc 121:233
33. Sobkowski J, Czerwiński A (1974) J Electroanal Chem 55:391
34. Czerwiński A, Sobkowski J, Więckowski A (1974) Int J Appl Radiat Isot 25:295
35. Czerwiński A, Sobkowski J (1975) J Electroanal Chem 59:41
36. Sobkowski J, Czerwiński A (1975) J Electroanal Chem 65:327
37. Czerwinski A (1988) J Electroanal Chem 252:189
38. Waszczuk P, Wieckowski A, Zelenay P, Gottesfeld S, Coutanceau C, Leger J-M, Lamy C (2001) J Electroanal Chem 511:55
39. Breiter MW (1967) Electrochim Acta 12:1213
40. Willsau J, Heitbaum J (1986) Electrochim Acta 31:943
41. Brisard GM, Camargo APM, Nart FC, Iwasita T (2001) Electrochem Commun 3:603
42. Babu PK, Tong YY, Kim HS, Wieckowski A (2002) J Electroanal Chem 524–525:157
43. Babu PK, Kim HS, Oldfield E, Wieckowski A (2003) J Phys Chem B 107:7595
44. Lagutchev A, Lu GQ, Takeshita T, Dlott DD, Wieckowski A (2006) J Chem Phys 125:154705
45. Łukaszewski M, Czerwiński A (2006) Electrochim Acta 51:4728
46. Łukaszewski M, Czerwiński A (2007) J Electroanal Chem 606:117
47. Siwek H, Łukaszewski M, Czerwiński A (2008) Phys Chem Chem Phys 10:3752
48. Frelink T, Visscher W, van Veen JAR (1996) Langmuir 12:3702
49. Jusys Z, Massong H, Baltruschat H (1999) J Electrochem Soc 146 (3):1093
50. Hachkar M, Napporn T, Léger J-M, Beden B, Lamy C (1996) Electrochim Acta 41:2721
51. Visscher W, Gootzen JFE, Cox AP, van Veen JAR (1998) Electrochim Acta 43:533
52. Stalnionis G, Tamašauskaitė-Tamašiūnaitė L, Pautienienė V, Jusys Z (2006) J Electroanal Chem 590:198
53. Siwek H (2008) PhD Thesis, Warsaw University
54. Łukaszewski M, Czerwiński A (2006) J Electroanal Chem 589:38
55. Łukaszewski M, Czerwiński A (2009) J Alloys Compd 473:220
56. Sauerbrey G (1959) Z Phys 155:206
57. Rand DAJ, Woods R (1672) Electroanal Chem 36:57
58. Woods R (1976) Chemisorption at Electrodes. In: Bard AJ (ed) Electroanalytical chemistry, vol 9. Marcel Dekker, New York, p 2
59. Aston MK, Rand DAJ, Woods R (1984) J Electroanal Chem 163:199
60. Capon A, Parsons R (1975) J Electroanal Chem 65:285
61. Kadirgan F, Beden B, Leger J-M, Lamy C (1981) J Electroanal Chem 125:89
62. Siwek H, Tokarz W, Piela P, Czerwiński A (2008) J Power Sources 181:24
63. Tokarz W, Siwek H, Piela P, Czerwiński A (2007) Electrochim Acta 52:5565
64. Sobkowski J, Więckowski A, Zelenay P, Czerwiński A (1979) J Electroanal Chem 100:781
65. Angelucci CA, Nart FC, Herrero E, Feliu JM (2007) Electrochem Commun 9:1113
66. Santos MC, Miwa DW, Machado SAS (2000) Electrochem Commun 2:692
67. Wasberg M, Bácskai J, Inzelt G, Horányi G (1996) J Electroanal Chem 418:195
68. Kolics A, Wieckowski A (2001) J Phys Chem B 105:2588
69. Łukaszewski M, Siwek H, Czerwiński A (2007) Electrochim Acta 52:4560
70. Jerkiewicz G, Vatankhah G, Lessard J, Soriaga MP, Park Y-S (2004) Electrochim Acta 49:1451
71. Kunimatsu K, Samant MG, Seki H (1989) J Electroanal Chem 258:163
72. Osawa M, Tsushima M, Mogami H, Samjeské G, Yamakata A (2008) J Phys Chem C 112:4248
73. Hepel M (1998) J Electrochem Soc 145:124